Detection of hydrated electrons in water-jet immersed in low-pressure plasma by laser-induced desolvation

Yoshinobu Inagaki‡ and Koichi Sasaki§

Division of Applied Quantum Science and Engineering, Hokkaido University, Sapporo 060-8628, Japan

E-mail: sasaki@qe.eng.hokudai.ac.jp

Abstract. We detected hydrated electrons in a micrometer-size water jet immersed in a low-pressure plasma by laser-induced desolvation. When we irradiated the 2nd, 3rd, and 4th harmonics of Nd:YAG laser pulses to the water jet, we detected the pulsed current which indicated the transport of electrons from the water jet to the plasma. We observed a proportional relationship between the amplitude of the pulsed current and the laser energy, which is consistent with the conversion from hydrated to free electrons by laser-induced desolvation. The amplitude of the pulsed current increased with the negative bias voltage between the plasma and the water jet. The most remarkable result was found in the relationship between the photon energy and the quantum yield of the electron transport. The experimental quantum yield was orders of magnitude higher than that predicted by a Monte Carlo simulation in a low photon energy region, suggesting the possibility that hydrated electrons we detected in the present experiment have much lower hydration energies than well-known hydrated electrons.

1. Introduction

With the increased demand on the understanding of reaction mechanisms in new plasma applications, such as water treatment, medicine, agriculture, and analysis [1–8], many diagnostic techniques for plasma-liquid (water) interactions have been developed. In particular, in recent several years, the diagnostics of the narrow region just below the plasma-liquid interface attracts much attention of many researchers, since high densities are expected for short-lived reactive species in the interfacial region. One of short-lived reactive species induced by plasma-water interaction is the solvated (hydrated) electron. The solvated electron is a metastable electron surrounded by polar solvent molecules. After the discovery of the hydrated electron in 1962 [9], the rate constants for reactions with various chemicals have been investigated by pulse radiolysis and flash photolysis [10–12]. However, the pulse radiolysis and the flash photolysis examined the reactivity of hydrated electrons in bulk water, and there would be a possibility that hydrated electrons located in the interfacial region have different reactivity.

‡ Present address: Institute for Catalysis, Hokkaido University
§ Author to whom any correspondence should be addressed.

The hydrated electron is known to be a strong reducing agent [13], and it surely plays an important role in plasma-liquid (water) interaction [14]. However, the experimental investigation on reaction processes of hydrated electrons in the plasma-water interaction is seriously insufficient to date. The limited number of experimental investigation is owing to the lack of diagnostic techniques to detect hydrated electrons just below the plasma-water interface. The first detection of hydrated electrons in the interfacial region between water and an atmospheric-pressure plasma was reported by Rumbach and coworkers in 2015 [15]. They adopted laser absorption spectroscopy with the total reflection geometry to the water that worked as the anode of an atmospheric-pressure dc glow discharge. We presume that it is a delicate experiment, since the water electrode usually fluctuates during the discharge [16,17]. Recently, we developed another method to detect hydrated electrons in the interfacial region [18]. The method is based on laser-induced desolvation, where hydrated electrons in the interfacial region are converted to free electrons by the irradiation of a laser beam having a photon energy exceeding the hydration energy. Free electrons produced by desolvation are transported to the gas phase. In a previous work [18], we employed an atmospheric-pressure dc glow discharge where the water surface worked as the cathode. We observed the pulsed increase in the discharge current, which was caused by the transport of free electrons from the water to the plasma, at the timing when the water cathode was irradiated with the laser pulse.

A limitation in our previous experiment is caused by the fact that the water works as the cathode of the dc discharge. In this case, the water surface is irradiated by positive ions only, and the energies of positive ions are not predictable since the cathode sheath is highly collisional at the atmospheric pressure. However, the experiment of laser-induced desolvation with the inverted polarity is impossible, since free electrons produced from hydrated electrons cannot pass through the discharge circuit if the water works as the anode of the discharge. In other words, laser-induced desolvation is not compatible with the irradiation of electrons onto the water surface, if we employ a dc discharge for the experiment.

To overcome the difficulty, in the present work, we injected a micrometer-size water jet into a low-pressure inductively coupled plasma [19, 20]. The plasma potential is determined by the potential of the chamber wall in the inductively coupled plasma source, and the potential difference between the plasma and the water jet is controllable by the bias voltage applied to the water jet. If the potential of the water jet is slightly lower than the plasma potential, free electrons produced by laser-induced desolvation can be transported to the plasma, even though the flux of electrons from the plasma is greater than that of positive ions. In addition, the energy of positive ions is determined by the bias voltage since we can assume a collisionless sheath. We examined the quantum yield of the electron transport caused by laser-induced desolvation in the water jet. As as result, we found that the quantum yield observed in the present experiment was much higher than that observed in the atmospheric-pressure dc discharge with the water cathode [18]. In addition, the quantum yield was orders of magnitude higher than that predicted by a Monte Carlo simulation at a low photon energy, suggesting the possibility that hydrated electrons we detected in the present experiment have much lower hydration energies than well-known hydrated electrons.

2. Experimental method

Figure 1 shows a schematic of the experimental setup. An NaOH aqueous solution was squirted through a plastic (polyetheretherketone: PEEK) tube from the top of a vacuum chamber at a flow rate of 1.8 mL/min. The reason for choosing NaOH as the solute was its high electrical conductivity (Although some acids have higher conductivities, they damage the water-jet pump). The length and the inner diameter of the PEEK tube were 1.5 cm and 75 μm, respectively. The concentration of the NaOH solution was 10 %, which gave us the maximum electrical conductivity of 35 S/m. This conductivity resulted in a resistance of 50 kΩ between the reservoir and the inlet of the PEEK tube, whereas the resistance of the solution inside the narrow PEEK tube was 100 kΩ. A double plunger pump was used for pressurizing the solution inside the PEEK tube, and the NaOH solution was ejected from the nozzle in the form of a jet. The plunger pump was electrically floating using an isolation transformer. The water jet had a filament-like shape with a length of approximately 2 cm in vacuum, and it was dispersed into droplets in the downstream. The body of the water jet did not reach the chamber wall. The droplets were caught on the bottom chamber which was cooled with liquid nitrogen. In addition, we installed a water vapor trap at the temperature of liquid nitrogen to reduce the pressure of water vapor in the chamber. The pressure of water vapor in the chamber was 7-9 mTorr. We added helium into water vapor, and the total pressure was 100 mTorr. An inductively coupled plasma was generated using a spiral antenna which was wound around a glass tube with a diameter of 8.5 cm. The antenna was connected to an rf power supply with a power of 150 W. The body of the water jet was irradiated with the 2nd, 3rd and 4th harmonics of Nd:YAG laser pulses. The durations of the laser pulses were 8 ns. The laser beam was not focused and its diameter was approximately 8 mm. The laser beam irradiated the top part of the water jet, and the center of the laser beam was placed at a distance of 4 mm from the nozzle. A dc voltage was applied between the electrical ground and the solution in the reservoir. The dc voltage was adjusted between -150 and +200 V. A coaxial cable was connected to the stainless-steel joint which held the PEEK tube, and the waveform of the pulsed voltage across the resistor of 50 Ω was recorded using an oscilloscope. The 50 Ω resistor and the oscilloscope were isolated from the dc bias circuit using a capacitor of 10 nF.

3. Results

3.1. Estimation of water jet potential

The NaOH solution used for the water jet had an electrical conductivity of 35 S/m, corresponding to 65 kΩ/cm for the resistance of the water jet that had a narrow diameter of 75 μm. Therefore, the potential of the water jet had a gradient along the axis when an electrical current passed through. We estimated the potential distribution of the water jet using the model shown in Fig. 2, where $V(z)$ is the potential of the water jet at a distance z from the end of the nozzle, $I(z)$ is the current along the water jet, and $J(z)$ is the current density passing from the water jet to the plasma. $J(z)$ is a function of $V(z)$. We assumed the relationship shown in Fig. 3 between $J(z)$ and $V(z)$, which is the ideal voltage-current

characteristic of a Langmuir probe. We adopted 1×10^{16} m^{-3}, 7 eV, and 30 V in Fig. 3 for the electron density, the electron temperature, and the plasma potential, respectively, on the basis of their measurements. We ignored the expansion of the sheath in this model, and the electron saturation current was assumed to be constant. Under the assumptions, the Kirchhoff's laws are given by

$$\frac{\mathrm{d}I(z)}{\mathrm{d}z} = -J(z)\pi d \tag{1}$$

and

$$\frac{\mathrm{d}V(z)}{\mathrm{d}z} = -I(z)r_{\mathrm{w}} \tag{2}$$

with the boundary conditions

$$V_0 = V_{\mathrm{dc}} - I_0 R_{\mathrm{path}} \tag{3}$$

and

$$I(L) = J(L)\frac{\pi d^2}{4}, \tag{4}$$

where d is the diameter of the water jet ($d = 75$ μm), L is the length of the water jet body ($L = 2$ cm), V_{dc} is the voltage of the dc power supply, $V_0 = V(0)$ and $I_0 = I(0)$ are the potential and the dc current at the nozzle, respectively, r_{w} is the resistance of the NaOH solution per the unit length of the water jet ($r_{\mathrm{w}} = 65$ kΩ/cm), and R_{path} is the resistance of the NaOH solution between the dc power supply and the nozzle ($R_{\mathrm{path}} = 150$ kΩ). We calculated $V(z)$ and $I(z)$ by solving Eqs. (1) and (2) numerically, by referring to the boundary conditions (Eqs. (3) and (4)) and the relationship between $V(z)$ and $J(z)$ shown in Fig. 3.

Figure 4 shows the comparison between the experiment and the calculation for the relationship between V_{dc} and I_0. The curves are rather similar to the voltage-current characteristics of a Langmuir probe, but it is noted that V_{dc} is different from $V(z)$ due to the voltage drop along the NaOH solution. The rough agreement between the experiment and the calculation indicates the validity of the model shown in Fig. 2. On the basis of the validity of the model, we estimated the axial distribution of the water jet potential. As shown in Fig. 5, $V_0 \simeq V_{\mathrm{dc}}$ when V_{dc} was much lower than the plasma potential, and $V(z)$ was almost constant along the axis of the water jet. This was because the voltage drop along the NaOH solution was negligible at the small ion saturation current. In contrast, when V_{dc} was higher than or close to the plasma potential, $V(z)$ was much lower than V_{dc}, and $V(z)$ dropped sharply in the region close to the nozzle ($z \leq 0.5$ cm). The voltage drop was owing to the fact that the electron current was much higher than the ion current in the voltage-current characteristics of the Langmuir probe shown in Fig. 3. Therefore, the potential of almost all the part of the water jet was estimated to be lower than the plasma potential in the present experimental condition, even if we applied $V_{\mathrm{dc}} = +200$ V to the NaOH solution.

3.2. Pulsed current induced by laser irradiation

Figure 6 shows the waveform of the pulsed current observed by the irradiation of the Nd:YAG laser pulse onto the water jet. The laser energy and the wavelength were 30 mJ/pulse and 266

nm, respectively. The dc voltage applied to the NaOH solution in the reservoir was $V_{\rm dc} = 0$ V, namely, the water jet potential was negative with respect to the plasma potential. When the water jet was immersed in the plasma, we observed the pulsed current at the timing of the laser irradiation. The positive current means the electron transport from the water jet to the plasma, indicating the production of free electrons around the surface of the water jet. The width of the pulsed current was approximately 8 ns, which agreed with the duration of the laser pulse. The electron charge transported from the water jet was 7.14 pC, which was obtained by integrating the pulsed waveform over the time. The waveform of the pulsed current was roughly the same at various experimental conditions. For comparison, the waveform when the water jet was not immersed in the plasma is also shown in Fig. 6. A weak pulsed current was observed, of which the amplitude was less than 3% of the pulsed current when the water jet was immersed in the plasma. The amplitude of the pulsed current is plotted in Fig. 7 as a function of the energy of the 4th harmonics of the Nd:YAG laser pulse. The dc voltage applied to the NaOH solution was $V_{\rm dc} = 0$ V. As shown in Fig. 7, the amplitude of the pulsed current was roughly proportional to the laser energy. Figure 8 shows the relationship between the amplitude of the pulsed current and $V_{\rm dc}$. The water jet potential at a distance of 4 mm from the nozzle, which was estimated by the calculation described in Sec. 3.1, is indicated on the upper horizontal axis. Note that the upper horizontal axis shows the water jet potential at the center of the laser beam with a diameter of 8 mm. The amplitude of the pulsed current increased with the absolute value of the water jet potential, when the NaOH solution was biased negatively. On the other hand, if the NaOH solution was biased positively, the amplitude of the pulsed current was insensitive to the dc voltage. Note that the water jet potential was also insensitive to the dc voltage in the positive-bias case, which is seen from the upper horizontal axis of Fig. 8. In addition, it is also noted that the ejection of free electrons was blocked at the top part ($z \leq 0.3$ cm) of the water jet if the NaOH solution was biased at $V_{\rm dc} = +200$ V, since the potential of the part was higher than the plasma potential.

3.3. Effect of photon energy

The amplitude of the pulsed current is shown in Fig. 9 as a function of the photon energy. The dc bias voltage was $V_{\rm dc} = 0$ V. The laser energies were adjusted to 12, 9, and 6 mJ/pulse at the wavelengths of 266, 355, and 532 nm, respectively, which enabled us to carry out the experiments with the same photon flux at the different photon energies. We also plotted our previous data observed in an atmospheric-pressure dc glow discharge (APGD), where the plasma-liquid interface worked as the cathode (the plasma-liquid interface was bombarded by positive ions) [18]. The solid curves show the relative quantum yield estimated by the Monte Carlo simulation [18]. The details of the Monte Carlo simulation have been described in the previous paper. The quantum yield means the number of electrons ejected from the plasma-liquid interface by the irradiation of one photon, and the pulsed current observed experimentally is proportional to the quantum yield. Since the distance between the birth place of free electrons and the solution surface affects the transport efficiency significantly, we assumed two locations (0.1 and 9 nm from the solution surface) for the birth place, where

hydrated electrons are converted to free electrons by laser-induced desolvation. All the plots and the curves are normalized at the photon energy of 4.66 eV (266 nm). As shown in Fig. 9, the experimental results observed in APGD indicate that the location of hydrated electrons is at a distance of 9 nm from the solution surface [18]. On the other hand, the quantum yield observed in the present experiment was remarkably different from that observed in APGD, and the relationship between the quantum yield and the photon energy was not explained by the simulation even if we assumed 0.1 nm for the distance between the location of hydrated electrons and the solution surface.

4. Discussion

4.1. Validity of experiment

Since water vapor is an electronegative gas, it is possible that negative charges in the plasma are composed of electrons and negative ions. In this case, photodetachment produces additional electrons from negative ions in the plasma by the irradiation of the Nd:YAG laser pulses, since the photon energies are higher than the thresholds of photodetachment for OH^- [21], O^- [22, 23], and H^- [24, 25]. If the potential of the water jet is higher than or close to the plasma potential, electrons produced by photodetachment are transported from the plasma to the water jet. Since the direction of the electron transport due to photodetachment is opposite to that due to laser-induced desolvation, the signal of laser-induced desolvation is possibly cancelled out. We examined the influence of negative ions by employing an apparatus of probe-assisted laser photodetachment [26, 27]. A cylindrical Langmuir probe having a steinless-steel tip with a diameter of 1 mm and a length of 8 mm was inserted into the plasma. The probe was connected to the electrical ground via a dc power supply at +70 V and a resistor of 50 Ω. The potential of +70 V was higher than the plasma potential. The probe was irradiated with the Nd:YAG laser pulses, and the pulsed voltage across the resistor was recorded using an oscilloscope. The laser energy and the wavelength were 30 mJ/pulse and 266 nm, respectively. As a result, we observed that the pulsed current at the timing of the pulsed laser irradiation was lower than the detection limit. As has been mentioned in Sec. 3.2, we detected clear pulsed current showing the electron transport from the water jet to the plasma, when the water jet was irradiated with the Nd:YAG laser pulses. Therefore, we concluded that photodetachment of negative ions in the plasma did not affect the detection of hydrated electrons by laser-induced desolvation.

Negative ions exist in the NaOH solution at their solvated states. However, they do not affect the measurements since the solvation energies of negative ions in the solution are higher than the photon energies of the Nd:YAG lasers. Although the charge transfer to solvent (CTTS) transition reduces the photon energy that is necessary to induce photodetachment of negative ions, 6.2-6.7 eV is necessary for the CTTS transition of OH^- [28]. Hence, the production of free electrons from negative ions is impossible in the solution. Therefore, laser-induced desolvation of hydrated electrons is only the process that can produce free electrons in the experimental condition.

The proportional relationship between the laser energy and the amplitude of the pulsed current, which is shown in Fig. 7, supports the validity of the experiment, since laser-induced desolvation is a one-photon process. If the water jet potential exceeds the plasma potential, free electrons produced via laser-induced desolvation are not transported to the plasma. However, the water jet potential do not exceed the plasma potential except the top part of the nozzle with $V_{\rm dc} = +200$ V, as shown in Fig. 5. Therefore, we believe that the amplitude of the pulsed current observed in the present experiment represents the amount of free electrons ejected from the plasma-liquid interface, or the relative quantum yield of laser-induced desolvation.

4.2. Kinetics of hydrated electrons

There are two possible processes for the production of hydrated electrons in the present experimental condition. One is the direct hydration of free electrons transported from the plasma and the other is the hydration of electrons produced by ion impact ionization of liquid H_2O. These two production processes are switched by the potential of the water jet. When the water jet has a deep negative potential with respect to the plasma potential, the electron flux is negligibly low and the water jet is irradiated by positive ions only. In this case, the origin of hydrated electrons is ion impact ionization of water molecules, and it is expected that the production rate increases with the absolute value of the negative water jet potential or the positive ion energy. The experimental result shown in Fig. 8 for $V_{\rm dc} \leq 0$ V is consistent with this expectation. The rate of ion impact ionization decreases with $V_{\rm dc}$, and it becomes negligible if the potential difference between the water jet and the plasma is lower than the ionization potential of H_2O (12.6 eV) [29]. On the other hand, the electron flux exceeds the ion flux if the water jet potential is higher than the floating potential, and in this case, the direct hydration of free electrons transported from the plasma can work as the production process. The electron flux increased with $V_{\rm dc}$, as shown in Fig. 4. However, the hydrated electron density was insensitive to $V_{\rm dc}$, as shown in Fig. 8. The increase in the hydrated electron density for $V_{\rm dc} \geq 0$ V was too slight even if considering the fact that the top part of the water jet had a higher potential than the plasma potential at $V_{\rm dc} \simeq +200$ V. Since the increase in the electron flux with $V_{\rm dc}$ is sure, as shown in Fig. 4, the almost constant hydrated electron density is attributed to the destruction process. Rumbach and coworkers reported the destruction of hydrated electrons by $\mathrm{e^-_{solv}} + \mathrm{e^-_{solv}} \rightarrow \mathrm{H_2} + 2\mathrm{OH^-}$ in water interacting with an atmospheric-pressure plasma [15]. The rate coefficient of this reaction is 1.1×10^{10} $\mathrm{M^{-1}s^{-1}}$ [13]. If this reaction is the dominant destruction process in our experimental condition, the amplitude of the pulsed current is proportional to the square root of the positive dc current. However, the dependence of the amplitude of the pulsed current on the positive dc current was weaker than the square root relationship, suggesting the contribution of other destruction processes. A possible destruction process is the reaction with $\mathrm{O^{\cdot -}}$. Tochikubo and coworkers have reported the production of $\mathrm{OH^{\cdot}}$ by collision between liquid H_2O and free electron via dissociative electron attachment and dissociative deexcitation of $\mathrm{H_2O^*}$ [30,31]. In the solution with a high pH value, $\mathrm{OH^{\cdot}}$ is converted to $\mathrm{O^{\cdot -}}$ via $\mathrm{OH^{\cdot}} + \mathrm{OH^-} \leftrightarrow \mathrm{O^{\cdot -}} + \mathrm{H_2O}$ immediately. It is known

that hydrated electron reacts with $O^{\cdot -}$ with a rate coefficient of 2.2×10^{10} $M^{-1}s^{-1}$ [13]. This is a possible mechanism of the insensitive dependence of the amplitude of the pulsed current on the dc current for $V_{\rm dc} \geq 0$ V, but further investigation is necessary to obtain the full understanding of the kinetics of hydrated electrons.

4.3. Possibility of partially hydrated electrons

The most important finding obtained by the present experiment is included in Fig. 9, which shows the significant discrepancy between the experimental result and the Monte Carlo simulation. As described in the previous paper [18], the experimental result observed in APGD was reproduced by the simulation if we assumed that hydrated electrons were located at a distance of 9 nm from the plasma-liquid interface. However, we also pointed out that the experimental quantum yield was higher than that in the simulation at photon energies below 3.8 eV. The quantum yield observed in the present experiment at a photon energy of 3.5 eV was much higher than that observed in APGD, and it is not explained by the simulation even if we assume that hydrated electrons are located at the top surface of the solution (0.1 nm).

It should be emphasized here that we assume the solvation energy reported by Suzuki and coworkers [32] in the simulation. It has a Gaussian distribution with the center at 3.76 eV and the standard deviation of 0.43 eV. The photon energy dependence of the relative quantum yield suggests that the solvation energy of hydrated electrons detected in the present experiment is lower than that reported by Suzuki and coworkers [32]. The possibility of a hydrated electron with a lower solvation energy, which is called partially hydrated electron, has been reported by several authors [33, 34]. It is presumed that partially hydrated electron is surrounded by a smaller number of water molecules than fully hydrated electron, and it can exist at a short distance ($\sim$ 3 nm) from the gas-liquid interface. Hydrated electrons are produced by the irradiations of electrons and ions in the case of plasma-liquid interaction, and the production rate of hydrated electrons are high in the vicinity of the plasma-liquid interface. Therefore, partially hydrated electrons are realistic in plasma-liquid interaction. The smaller amount of partially hydrated electrons in the experiment using APGD may be explained by the higher destruction rate due to higher densities of reactive species in the interfacial region. Since the densities of reactive species are lower in the low-pressure plasma than the atmospheric-pressure plasma, partially hydrated electrons can survive in the interfacial region and they are detected by laser-induced desolvation at the low photon energy. Note that the result shown in Fig. 9 does not argue the domination of partially hydrated electrons. Since laser-induced desolvation has a higher sensitivity to hydrated electrons located at a shorter distance from the plasma-liquid interface [18], the signal of fully hydrated electrons at a longer distance would be masked by partially hydrated electrons even if the density of fully hydrated electrons is higher than that of partially hydrated electrons.

5. Conclusions

In this work, we irradiated the 2nd, 3rd, and 4th harmonics of Nd:YAG laser pulses onto the jet of an NaOH solution immersed in a low-pressure plasma. Employing the water jet enabled us to carry out the experiment of laser-induced desolvation when the electron flux to the water is greater than the ion flux. We detected the pulsed current from the plasma to the water jet, indicating the transport of free electrons produced by laser-induced desolvation. The amplitude of the pulsed current increased with the absolute value of the negative water jet potential, suggesting the hydration of electrons produced by ion impact ionization of liquid H_2O. On the other hand, the amplitude of the pulsed current was roughly constant when the potential of the water jet was higher than the floating potential, indicating that the density of hydrated electrons was insensitive to the electron flux. The amplitudes of the pulsed currents observed at low photon energies (the 2nd and 3rd harmonics) were not explained by the solvation energy of fully hydrated electron. The experimental result suggests the possibility that hydrated electrons produced by plasma-liquid interaction have lower hydration energies than fully hydrated electrons.

Acknowledgments

The authors would like to thank Naoki Shirai for useful discussion. This work was supported by JSPS KAKENHI (21J11632, 20H00135, and 19K21861).

References

[1] Bruggeman P and Leys C 2009 *J. Phys. D: Appl. Phys.* **42** 053001
[2] Bruggeman P J, Kushner M J, Locke B R, Gardeniers J G E, Graham W G, Graves D B, Hofman-Caris R C H M, Maric D, Reid J P, Ceriani E, Fernandez Rivas D, Foster J E, Garrick S C, Gorbanev Y, Hamaguchi S, Iza F, Jablonowski H, Klimova E, Kolb J, Krcma F, Lukes P, Machala Z, Marinov I, Mariotti D, Mededovic Thagard S, Minakata D, Neyts E C, Pawlat J, Petrovic Z L, Pflieger R, Reuter S, Schram D C, Schröter S, Shiraiwa M, Tarabová B, Tsai P A, Verlet J R R, von Woedtke T, Wilson K R, Yasui K and Zvereva G 2016 *Plasma Sources Sci. Technol.* **25** 053002
[3] Locke B R, Sato M, Sunka P, Hoffmann M R and Chang J-S 2006 *Ind. Eng. Chem. Res.* **45** 882
[4] Fridman G, Friedman G, Gutsol A, Shekhter A B, Vasilets V N and Fridman A 2008 *Plasma Processes and Polymers* **5** 503
[5] Takaki K, Hayashi N, Wang D and Ohshima T 2019 *J. Phys. D: Appl. Phys.* **52** 473001
[6] Shirai N, Uchida S and Tochikubo F 2014 *Plasma Sources Sci. Technol.* **23** 054010
[7] Li X, Zhou S, Gao K, Ran J, Wu K and Jia P 2022 *IEEE Transactions on Plasma Science* **50** 1717
[8] Srivastava T, Simeni M S, Nayak G and Bruggeman P J 2022 *Plasma Sources Sci. Technol.* **31** 085010
[9] Hart E J and Boag J W 1962 *J. Am. Chem. Soc.* **84** 4090
[10] Barat F, Gilles L, Hickel B and Lesigne B 1972 *J. Phys. Chem.* **76** 302
[11] Elliot A J and Sopchyshyn F C 1984 *Int. J. Chem. Kinetics* **16** 1247
[12] Telser T and Schindewolf U 1986 *J. Phys. Chem.* **90** 5378
[13] Buxton G V, Greenstock C L, Helman W P and Ross A B 1988 *J. Phys. Chem. Ref. Data* **17** 513
[14] Elg D T, Delgado H E, Martin D C, Sankaran R M, Rumbach P, Bartels D M and Go D B 2021 *Spectrochimica Acta Part B: Atomic Spectroscopy* **186** 106307
[15] Rumbach P, Bartels D M, Sankaran R M and Go D B 2015 *Nat. Comm.* **6** 7248

[16] Shirai N, Ichinose K, Uchida S and Tochikubo F 2011 *Plasma Sources Sci. Technol.* **20** 034013
[17] Shirai N, Suga G and Sasaki K 2020 *Plasma Sources Sci. Technol.* **29** 025007
[18] Inagaki Y and Sasaki K 2022 *Plasma Sources Sci. Technol.* **31** 03LT02
[19] Ito T, Sakka T and Sasaki K 2022 *Plasma Sources Sci. Technol.* **31** 06LT02
[20] Faubel M, Schlemmer S and Toennies J P 1988 *Z Phys D - Atoms, Molecules and Clusters* **10** 269
[21] Schulz P A, Mead R D, Jones P L and Lineberger W C 1982 *The Journal of Chemical Physics* **77** 1153
[22] Burch D S, Smith S J and Branscomb L M 1958 *Phys. Rev.* **112** 171
[23] Génévriez M, Dunseath K M, Terao-Dunseath M, Hibbert A, Dochain A, Marion R and Urbain X 2018 *Phys. Rev. A* **98** 033410
[24] Smith S J and Burch D S 1959 *Phys. Rev.* **116** 1125
[25] Armstrong B H 1963 *Phys. Rev.* **131** 1132
[26] Hayashi D and Kadota K 1998 *J. Appl. Phys.* **83** 697
[27] Sirse N, Oudini N, Bendib A and Ellingboe A R 2016 *Plasma Sources Sci. Technol.* **25** 04LT01
[28] Jortner J, Raz B and Stein G 1961 *J. Chem. Phys.* **34** 1455
[29] Watanabe K and Jursa A S 1964 *J. Chem. Phys.* **41** 1650
[30] Tochikubo F, Shimokawa Y, Shirai N and Uchida S 2014 *Jpn. J. Appl. Phys.* **53** 126201
[31] Akiyama N, Nakagawa Y, Uchida S and Tochikubo F 2021 *J. App. Phys.* **129** 163304
[32] Nishitani J, Yamamoto Y, West C W, Karashima S and Suzuki T 2019 *Science Advances* **5** eaaw6896
[33] Siefermann K R, Liu Y, Lugovoy E, Link O, Faubel M, Buck U, Winter B and Abel B 2010 *Nature Chem.* **2** 274
[34] Matsuzaki K, Kusaka R, Nihonyanagi S, Yamaguchi S, Nagata T and Tahara T 2016 *J. Am. Chem. Soc.* **138** 7551

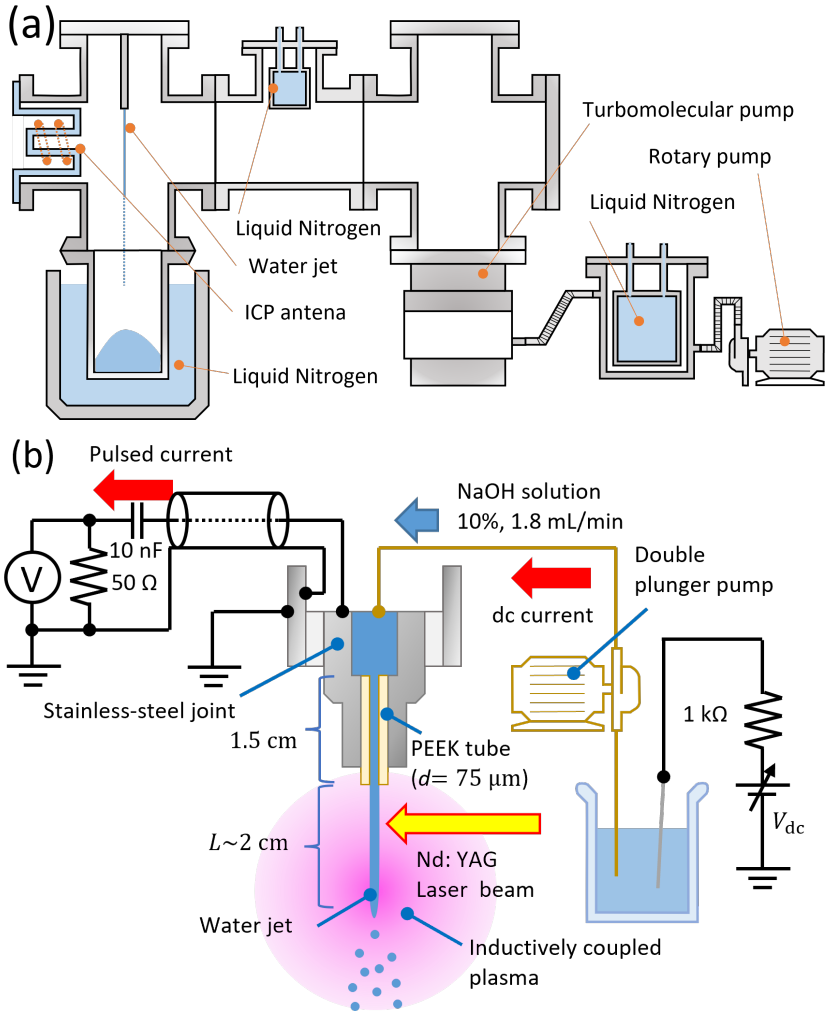

Figure 1. Schematic illustrations of (a) the whole the experimental apparatus and (b) the details around the water jet.

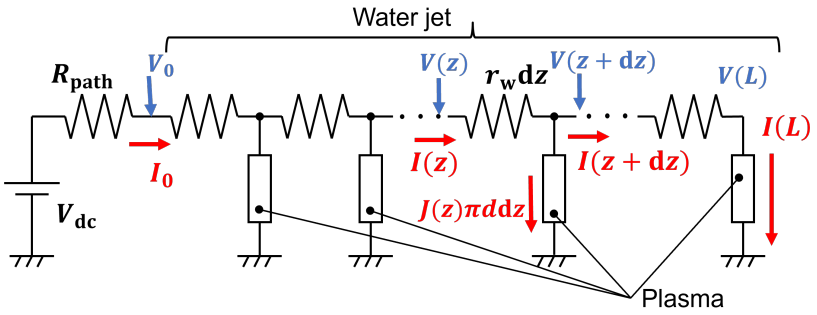

Figure 2. Circuit model used for calculating the distribution of the water jet potential.

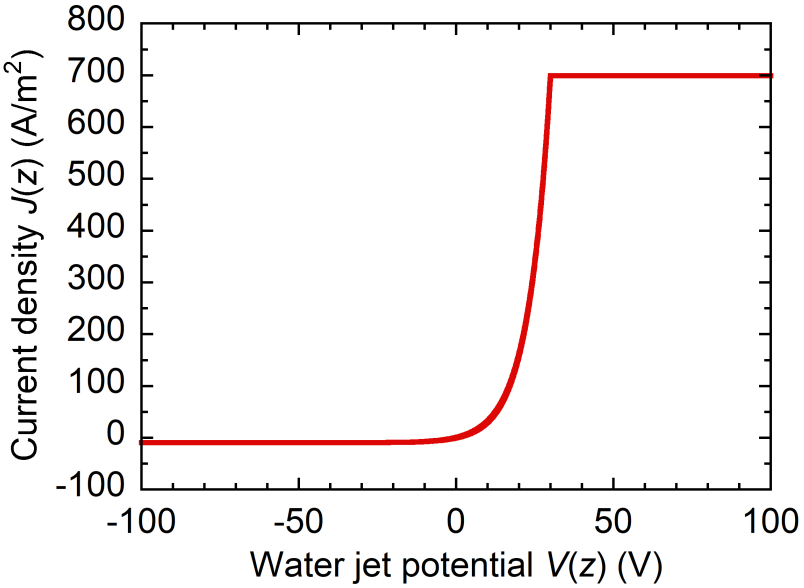

Figure 3. Relationship between $V(z)$ and $J(z)$ assumed in the circuit model calculation.

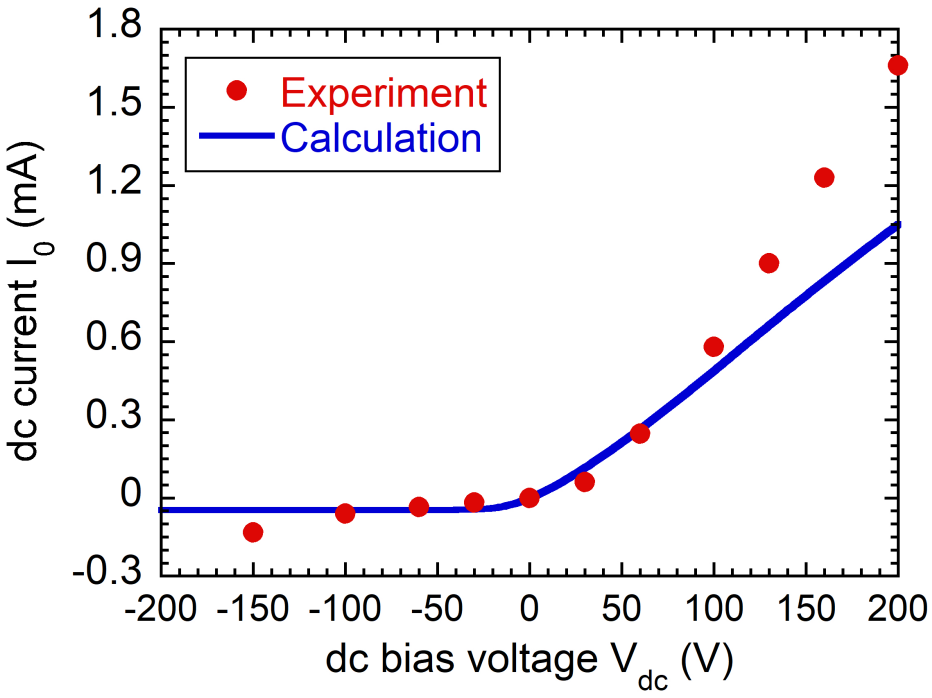

Figure 4. Comparison between the experiment and the circuit model calculation for the relationship between $V_{\rm dc}$ and I_0.

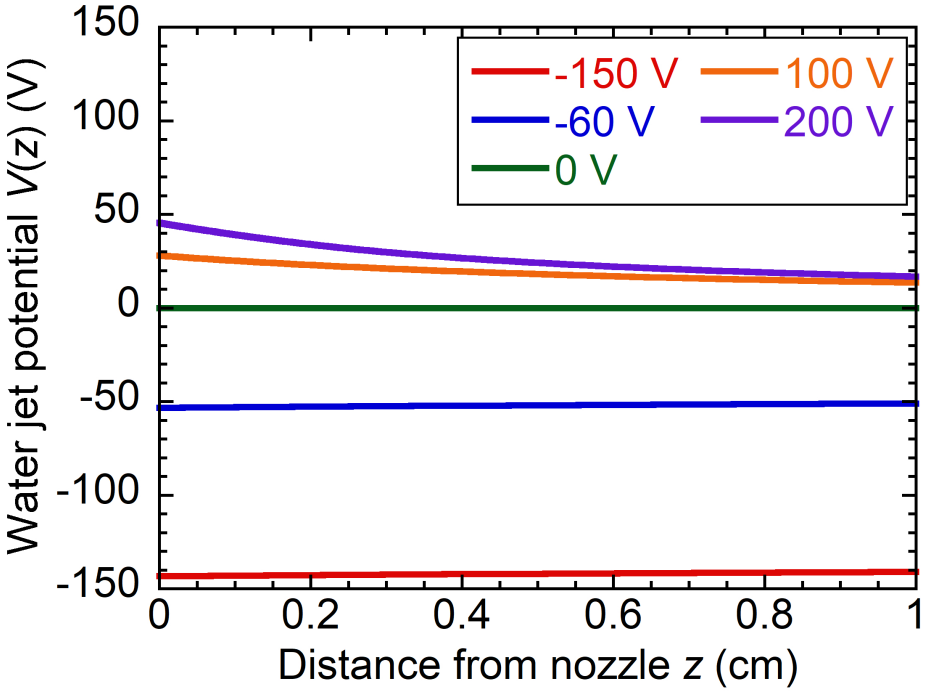

Figure 5. Axial distribution of the water jet potential estimated by the circuit model calculation at various V_{dc}.

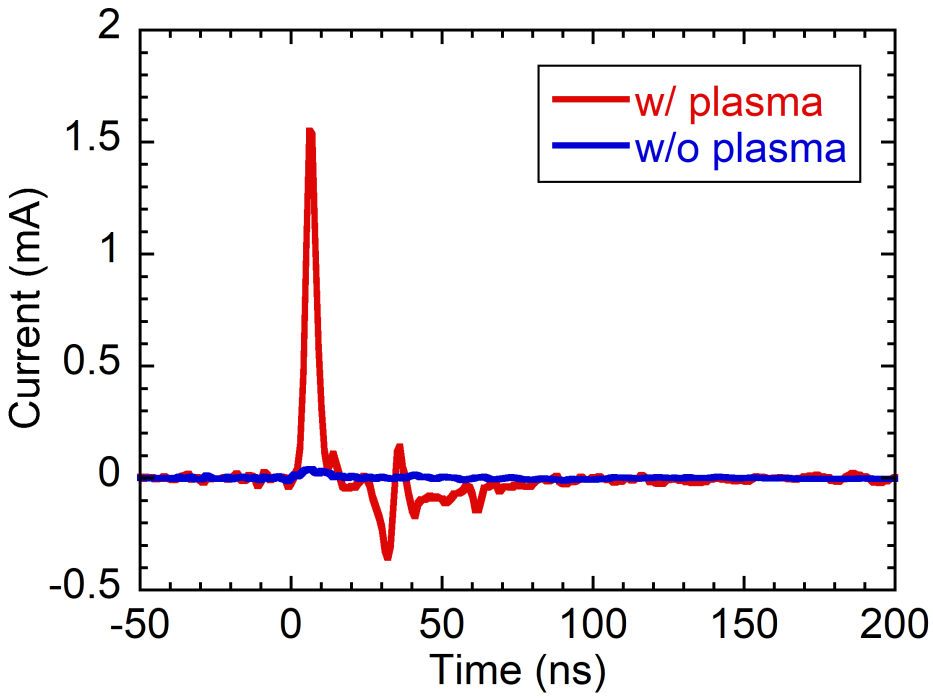

Figure 6. Waveform of the pulsed current observed by irradiating 4th harmonics of Nd:YAG laser pulse onto the water jet, which was immersed and was not immersed in the plasma. The positive current indicates the transport of electrons from the water jet to the plasma.

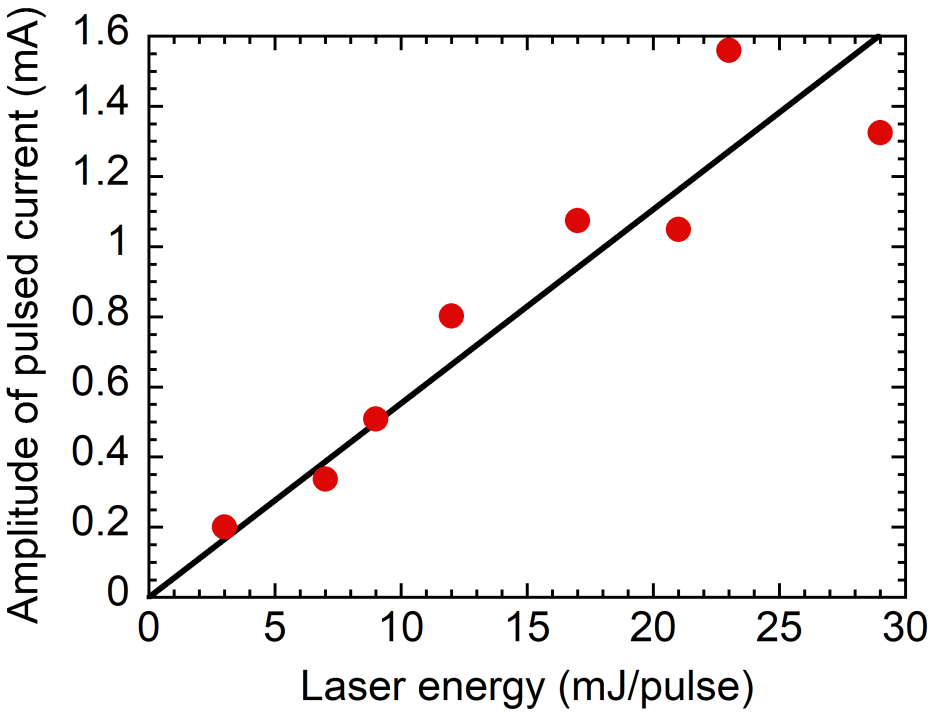

Figure 7. Amplitude of the pulsed current as a function of the energy of the Nd:YAG laser pulse at a wavelength of 266 nm.

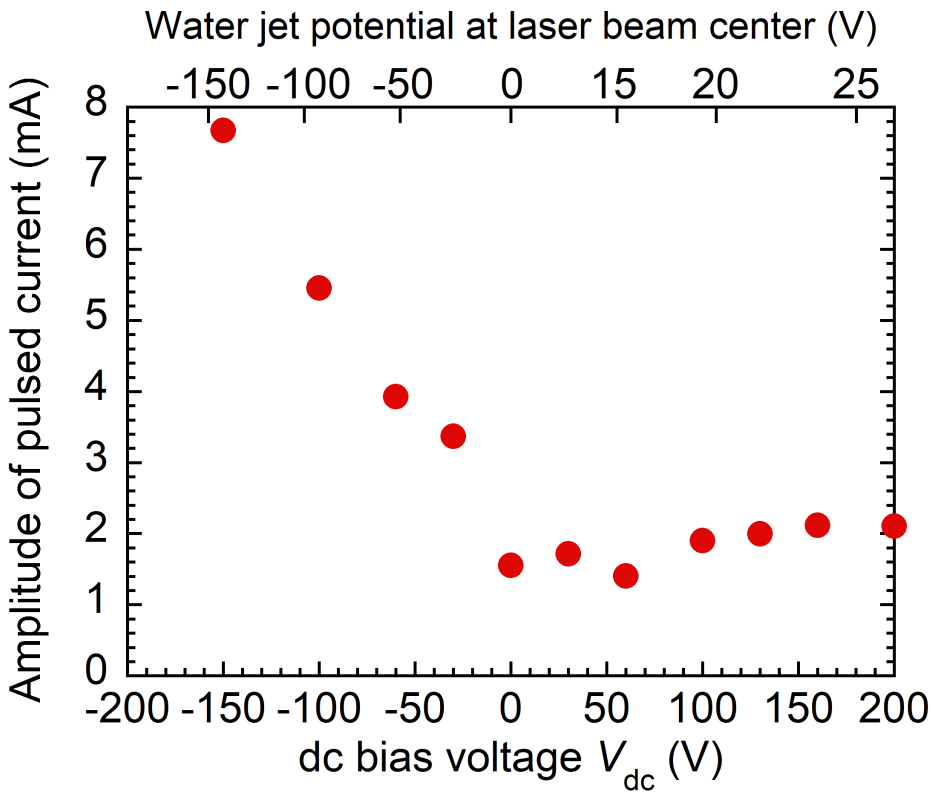

Figure 8. Amplitude of the pulsed current as a function of V_{dc}. The upper horizontal axis shows the water jet potential at the center of the Nd:YAG laser beam.

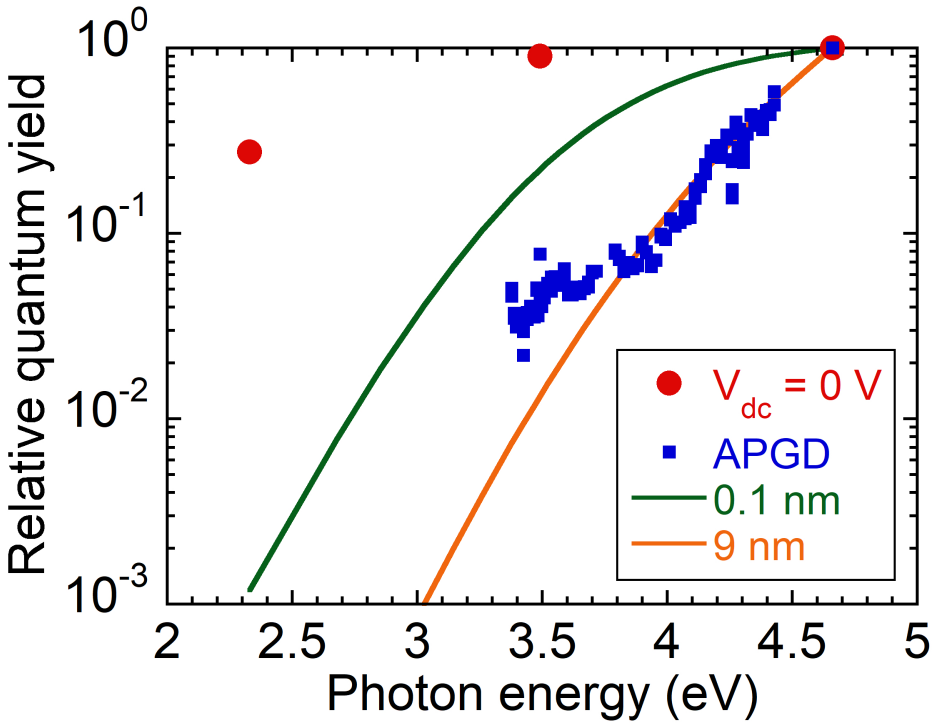

Figure 9. Relationship between the relative quantum yield of laser-induced desolvation and the photon energy of Nd:YAG laser pulses at the 2nd, 3rd, and 4th harmonics. The dc bias voltage applied to the water jet was $V_{\rm dc} = 0$ V. The results of the Monte Carlo simulation, where the locations of hydrated electrons are assumed to be 0.1 and 9 nm from the plasma-liquid interface, are also plotted. In addition, our previous experimental results observed in atmospheric-pressure dc glow discharge (APGD) [18] are also shown for comparison.